5th International Energy Conversion Engineering Conference and Exhibit (IECEC)
25 - 27 June 2007, St. Louis, Missouri

AIAA 2007-4740

A Magnetically-Actuated Resonant-Displacer Free-Piston Stirling Machine

Artin Der Minassians* and Seth R. Sanders†

EECS Department, University of California at Berkeley, Berkeley, CA, 94720, USA

Design, fabrication, and measurement results of a single-phase free-piston Stirling engine are presented in this paper. The engine has the potential to be expanded into a multiphase Stirling engine system. A very low-loss resonant displacer piston is designed for the system using a magnetic spring. Incorporating an array of permanent magnets, the magnetic spring has a very linear stiffness characteristic within the range of the displacer's stroke. The total power loss of the displacer piston at nominal conditions is less than 1 W. The power piston is not mechanically linked to the displacer piston and forms a mass-spring resonating subsystem with the gas spring and has resonant frequency matched to that of the displacer.

The design of heat exchangers are discussed with an emphasis on their low fluid friction losses. The heater and cooler are based on a fin-tube design fabricated by press-fitting tubes in a column of etched metal fins. The fabricated engine prototype is successfully tested as an engine and the experimental results are presented and discussed. Extensive experimentation on individual component subsystems confirms the theoretical models and design considerations.

I. Introduction

THERE has been an ongoing effort on low-cost solar-thermal-electric power generation technology in the EECS department at UC Berkeley over the past few years. The proposed energy conversion system is conceived to convert solar power into electricity in three stages: solar power to heat, heat to mechanical power, and mechanical power to electricity. Low-concentration nonimaging solar collectors are capable of delivering thermal power at temperatures in the range of 180 °C to 250 °C without having to track the sun.[1] A non-tracking system avoids the costs and maintenance issues associated with tracking collectors with high concentration ratios. Thus, a nonimaging solar collector is a very suitable component to serve as the first energy conversion stage of the proposed system.

A Stirling engine, in the proposed system, is utilized to convert the delivered heat by the solar concentrator into mechanical power. One potential advantage of the Stirling cycle is the possibility of using ambient air as the working fluid, and thus avoiding issues with long-term containment and the associated maintenance requirements. Further, recent success in demonstrating very low differential temperature engines is also compelling.[2] In the system conceived here, the Stirling engine converts moderate temperature heat to electricity by way of integrated electric generation. However, the use of low-temperature heat limits the theoretical maximum thermodynamic efficiency achievable by the heat engine, which limits the overall system efficiency. This disadvantage, however, can be compensated by lower costs in materials and in reduced maintenance. We take the view that cost effectiveness of solar electric technologies should be judged by output power per dollar rather than by efficiency or other merits.[3]

Our studies show that a multiphase free-piston Stirling engine system has the potential of being a suitable component in the proposed power generation technology.[3] In a multiphase Stirling engine system, each piston is double acting, and responsible for displacing the working fluid between hot and cold chambers as well as extracting the mechanical power from the thermodynamic cycle. The alpha-type Stirling engine is the most convenient arrangement for a multiphase system.[3] A three-phase prototype proved that gas spring hysteresis

*Ph.D. Candidate, EECS Department, 205 Cory Hall, Berkeley, CA, 94720. E-mail: artin@eecs.berkeley.edu
†Professor, EECS Department, 518 Cory Hall, Berkeley, CA, 94720. E-mail: sanders@eecs.berkeley.edu

loss is a critical dissipation source in low-temperature free-piston engines.[4] It is quadratically proportional to the engine compression ratio and should be carefully addressed in the design.[5] For a given geometry in an alpha-type engine, the compression ratio is a function of the phase delay between the compression and expansion pistons that is determined by the number of the phases. Therefore, in a multiphase system, the number of the phases should be chosen based on a reasonable balance between mechanical output power and efficiency, evaluated while considering gas spring hysteresis losses.

The design, fabrication and test results for a very low-loss resonant displacer piston and heat exchanger are discussed in this paper for a single-phase free-piston gamma-type Stirling engine prototype. The prototype design considers its potential expansion into a multiphase system after completion of all assessment tests and model confirmation. Therefore, certain constraints are placed for the present design, as discussed at various points below.

First, we present a concise description of the overall engine design and discuss the thermodynamic behavior of the engine through simulation results. Design of the displacer piston and the heat exchangers are presented next and are compared with measurements in detail. The final section presents the preliminary data recorded from the fabricated prototype engine while in operation to confirm the models and assumptions of the design stage.

II. System Design and Thermodynamic Simulation

Figure 1 shows the schematic diagram of the engine design which represents two pistons and one heat exchanger setup of the conceived system. The gas circuit of the displacer subsystem is closed by means of tubing in order to provide a closed engine chamber. Both displacer and power piston have identical dimensions. Of course, in single-phase operation, the power piston interacts with ambient pressure on one side and engine chamber pressure on the other. To facilitate tight clearance sealing, and thus minimal enthalpy loss, the power piston is located on the cold side of the engine.

The engine design parameters are tabulated in Table 1. The displacer piston shuttles the working fluid (ambient pressure air) between expansion and compression spaces at the operating frequency of 3 Hz. Furthermore, the mass of the power piston has been chosen such that it resonates with the gas spring at (or close to) the operating frequency. A dynamical simulation has been carried out using the Stirling engine adiabatic model.[5] Figure 2 shows the simulation results in terms of temperature and volume variations of the compression and expansion spaces as well as pressure variation of the engine chamber and the P-V diagram of the Stirling cycle. Based on this simulation, with 150 °C difference between hot and cold side average temperatures, the engine's indicated output power is about 23.8 W at 9.4% thermal efficiency.

In the sequel, we will discuss the design of the displacer piston and the heat exchanger subsystems in detail with an emphasis on the loss contribution of each element.

III. Design

A. Displacer Subsystem

The displacer is designed as a reciprocating piston that moves along a shaft with stroke of about 15 cm. It is in contact with hot gas (about 200 °C) at one end and cold gas (about 30 °C) at the other as shown in figure 3. Thus, in addition to enduring the higher temperature, the displacer body material should minimize the heat leakage path between hot and cold spaces. In order to fulfill both requirements, among high-temperature plastics, Teflon (Polytetrafluoroethylene) and PEEK (Polyetheretherketone) appear to be good candidates. Both materials endure temperatures of up to 250 °C, and have a low thermal conductivity (0.25 W/mK). The heat leakage through the displacer piston is expected to be about 2 W, if fabricated by either of these plastics. For its superior machinability properties and higher tensile strength, PEEK is selected as the material of choice for fabrication of the first displacer piston prototype.

The displacer piston is designed to resonate with a linear spring at the design frequency of operation (i.e., 3 Hz). Considering the limited life of mechanical springs and other challenges presented by these components, a design is carried out that utilizes magnetic springs to obviate mechanical failures and ensure long operation life. Permanent magnet arrays have been incorporated within the displacer piston to enable two magnetic functions: a magnetic spring and a linear motion magnetic actuator. As depicted in figure 3, the displacer magnet array interacts with two stationary magnetic arrays to provide a linear spring function,

Table 1. Engine thermodynamic design parameters.

Operating temperatures	T_h^{ave}: 448 K T_k^{ave}: 298 K
Indicated powers	Schmidt analysis Input: 75.1 W Output: 25.2 W adiabatic model Input: 253.6 W Output: 23.8 W
Heater	Housing volume: 210 cm^3 Porosity: 27.5% Hydraulic diameter: 0.6 mm Wetted area: 0.35 m^2
Cooler	Housing volume: 210 cm^3 Porosity: 23% Hydraulic diameter: 0.5 mm Wetted area: 0.37 m^2
Regenerator	Housing volume: 260 cm^3 Porosity: 63.4% Hydraulic diameter: 0.2 mm Wetted area: 1.9 m^2
Pistons	Diameter: 10 cm Stroke: 15 cm
Tubing	volume: 500 cm^3 Hydraulic diameter: 19 mm

which sets the mass-spring resonant frequency equal to the indicated frequency of operation. The displacer magnet array also interacts with a pair of stationary actuating coils to provide the actuation force required to control and sustain the resonant motion at its full excursion. To meet the above-mentioned thermal conditions, high coercivity 28/30 grade Sm-Co magnets have been designed in to provide thermal stability. Sm-Co permanent magnets can typically be used up to 300 °C, and have coercivity temperature coefficient of −0.2% per °C.

Due to the relative motion of the displacer piston with respect to the stationary cylinder and magnetic arrays, the piston and stationary components are exposed to alternating magnetic fields. Such magnetic fields generate eddy currents in any electrically conducting material, and hence, can significantly increase system losses. The choice of a non-conductive material completely obviates this phenomenon in the displacer body. Also, the high resistivity iron-powder ring is a proper solution as a component of the stationary magnet arrangement. On the contrary, Sm-Co magnets have high conductivity. Therefore, to minimize eddy losses, each magnet array is realized by separate pieces of block magnets in a circular pattern to prevent the formation of large eddy currents, mitigating corresponding potential losses. The realization of these arrangements is shown in figures 4 and 5.

Magnetic spring designs are mostly made for very small strokes (e.g., 0.5 cm).[6–8] All reported stiffness characteristics deviate from linear behavior at the two extremes of the stroke. In a nonlinear mass-spring system the resonant frequency is a function of the oscillation amplitude and may present serious challenges in tuning. Hence, in order to avoid complex tuning strategies, a stronger magnet section is added at the two end pieces of the stationary magnet setup to preserve the linear stiffness characteristic throughout the displacer piston stroke. Figure 5 shows how this idea is realized by implementing wider magnets to provide more magnetic flux. A nonlinear finite-element analysis program, COMSOL, is utilized to determine the forces on different components of this system. Figure 6 shows the computed force-displacement characteristic. The correlation coefficient of a linear regression fit to the data points is 0.999, which indicates a very linear

behavior throughout the extent of the displacer stroke.

An embedded linear motion ball bearing enables a low friction and smooth piston motion. However, exposure of steel bearing balls to the surrounding magnetic fields would impede rolling. Hence, steel balls are replaced by non-magnetic ceramic (Silicon Nitride) balls. An average coefficient of friction for a linear motion ball bearing is between 0.002 and 0.004. This means an average power dissipation of $0.05 - 0.1$ W for the nominal horizontal operating conditions of the displacer with a mass of about 2.9 kg.

The displacer cylinder has been fabricated out of PEEK as well. In addition to eliminating any potential eddy loss and allowing for minimal thermal leakage between hot and cold spaces, it is a good match with the piston in terms of thermal expansion considerations. Due to the small pressure difference between the two ends of the displacer piston, due to fluid flow pressure drop through heat exchangers and tubing, clearance sealing is an appropriate way of separating the hot and cold air. At a relatively large clearance of 0.010 in. for the displacer piston, the average enthalpy loss is less than 4 W for a nominal temperature differential of 150 °C. This is negligible compared to 300 W of required engine input heat. The enthalpy loss may be further reduced by considering a tighter displacer clearance, if necessary.

B. Heat Exchangers

The displacer task, in this design, is to pump the working fluid through the heat exchangers (heater, cooler, and regenerator) on one side and through the tubing that connects the cold side of the displacer cylinder to the compression space on the other. Fluid flow through all these components is an irreversible phenomenon that requires pumping power to overcome the viscous friction involved. This power is supplied as a fraction of the engine's available mechanical output power and, hence, should be minimized.

A well-designed heat exchanger maintains a reasonable balance between both temperature and pressure drops, it provides enough surface area to transfer the required heat to the working fluid with minimal temperature drop and, at the same time, introduces a low flow friction loss. Large temperature drops from heat exchanger surface to the working fluid cannot be tolerated in our design, due to low temperatures and tight temperature differentials. Fluid flow friction is strongly correlated with the fluid mass flow rate and hydraulic diameter of the heat exchanger.

Heater and cooler geometry, in our design, is based on a fin-tube structure that is fabricated by press-fitting tubes through stacks of properly etched metal fins, figure 7. The flow friction and heat transfer chracteristics for the heat exchangers are evaluated based on the cross-sectional mean velocity of the working fluid through each opening and the suggested empirical correlations in Refs. 9 and 10. All the correlations discussed in these references pertain to unidirectional steady flow. However, we anticipate that for the low frequencies, and hence low Reynolds numbers, one should not expect too much deviation from empirical correlations obtained for unidirectional flow regimes. Thus, with hydraulic diameter of about 0.5 mm, the design is optimized for lower frequencies with pumping power in the range of 0.2-0.8 W for the heater and cooler combined, and a temperature drop of 3-5 °C for each at nominal input thermal power of about 300 W.

The regenerator is a stack of woven wire screens with circular cross-section wire. For flow friction, several empirical correlations that are obtained from experiments on various fluids and operating conditions, have been compared in Ref. 11 and updated in Ref. 12. All discussed correlations are for steady flow conditions, except the one by Tanaka.[13] On the other hand, the predicted efficiency based on the Tanaka correlation is actually exceeded by experimental measurements.[13] Ref. 14 presents a different approach for pressure drop calculation through packed columns of woven-wire screen in oscillatory flow condition. The latter calculates higher fluid flow dissipation compared to that in Tanaka's methodology. Nevertheless, since the working fluid conditions reported in both references fit in the range of conditions for the Stirling engine design discussed here, we consider both correlations in our regenerator design computations. With hydraulic diameter of about 0.2 mm, the design requires a pumping power of about 1.3-2.5 W for the regenerator.

Finally, the tubing and fittings are analyzed analogously to the heater and cooler. The corresponding fluid flow dissipation is evaluated using the mean cross-sectional velocity of the fluid and correlations suggested in Ref. 10. It turns out that these losses contribute an additional 0.5-2 W to the total flow friction dissipation.

Table 2 summarizes the calculated power dissipation associated with the displacer piston, heat exchangers, and the tubing. Total displacer power loss is estimated to be in the range of 2.05-5.4 Watts.

C. Power Piston

Since this engine is designed to have the potential of being expanded into a multiphase system, the power piston dimensions (diameter, length, and stroke) are made identical to those of the displacer domensions. By enforcing such an arrangement, one can easily remove the tubing and convert this system into an alpha-type Stirling engine that is the most convenient arrangement for a multiphase Stirling engine system.

In this design, the power piston is located on the cold side of the engine. This eliminates any heat leakage in the form of thermal conduction through the piston body and facilitates tighter clearance sealing that is crucial in this case as the pressure difference across power piston may achieve 0.2 Bars, figure 2. Like the displacer, the power piston is moving along a shaft that goes through a linear motion ball bearing with non-magnetic balls that is embedded in the piston.

The power piston is the moving component of a magnetic circuit, similar to the displacer, that converts the output power of the thermodynamic cycle into electricity. The power piston is fabricated out of low-carbon steel with strong Nd-Fe-B permanent magnets installed on one end, figure 8. With a mass of 6.4 kg, the power piston resonates with the gas spring at the designed operating frequency. Although there is no need for additional springs, a small spring helps set the piston resting position in the midle of the shaft. By using a steel shaft we achieve that goal in our design. Since power piston will be delivering power to the load, it is a heavily damped (low quality factor, Q) component. Therefore, slight deviation of its resonant frequency is not expected to hinder the operation of the engine.

The linear motion ball bearing surface friction and eddy loss in the power piston body are the dissipation sources associated with this component. We rely on the friction factor that is experimentally obtained for the displacer ball bearing in the following section. The power piston weighs about 6.4 kg and, hence, the corresponding friction loss at full excursion is estimated to be about 1.25 W. Eddy losses are due to the variable magnetic field that is generated by the load current flowing through the coils. There is no precise estimation for eddy losses at this stage but they are not expected to be very high due to the relatively small load currents.

Due to the pressure differential across power piston, the working fluid will leak in and out through the clearance seal. Our simulation program predicts no more than 1 W dissipation through the wall clearance.

IV. Experimental Assessment

A. Displacer Piston

The only anticipated sources of dissipation in the displacer piston are the friction between the linear motion ball bearing and the shaft, and minor eddy losses in the permanent magnets and the iron powder cores. A ring-down test, among others, is an appropriate way for estimating the power dissipation of this system. The system is displaced from its equilibrium and is released. By observing the rate and type of the oscillation envelope (exponential for viscous friction or linear for dry friction,) one can translate it into important system parameters such as natural frequency, quality factor, and damping factor which are used to estimate the power loss.

Figure 9 shows the ring-down characteristic of the displacer piston by displaying open circuit actuator winding voltage. The very first peak coresponds to the maximum velocity of the piston (about 1.4 m/s). This test successfully confirms the expected 3 Hz resonant frequency and low power dissipation of the system. We are interested in analyzing the behavior of this system at the largest amplitudes as these are representative of the actual operating conditions. The ring-down envelope for larger amplitudes is clearly a straight line that signifies dry friction as the main source of loss. Note that the eddy loss would be characterized with an exponential envelope in a ring-down test. The estimated attenuation rate of the ring-down charactersitic is about 0.14 (m/s)/s which corresponds to a friction force of 0.6 N and about 0.5 W of power dissipation. This translates into a surface friction coefficient of 0.02 considering that the displacer piston weighs about 2.9 kg.

In order to verify the estimated power dissipation of the displacer piston, we implement the energy-balance approach. Utilizing only two phases of a three-phase inverter (DC to AC power converter,) alternating voltage is applied to the displacer actuating coils (see figure 3). Both amplitude and frequency of the alternating voltage can be adjusted by varying the inverter DC voltage or switching frequency. The frequency is adjusted to exactly match the resonant frequency obtained from the ring-down test and the DC voltage is increased until the nominal stroke is reached. By observing the terminal voltage and input current

waveforms, one can calculate the displacer piston dissipation (aggregate of surface friction, eddy loss, and fluid flow friction if present) by subtracting the coil copper loss from input power. Measured resistance and inductance of each coil is about 10.2 Ω and 145 mH, respectively. Figure 10 depicts the input voltage and current waveforms when the displacer is tested in absence of the heat exchangers and connecting tubes. In this case, the calculated input power and copper loss are 1.75 W (fundamental frequency power factor is 0.99) and 0.99 W, respectively. Consequently, it is inferred that 0.76 W supplies the losses in the displacer piston.

B. Heat Exchangers

Both ring-down and energy-balance tests are appropriate methods to assess the fluid flow friction losses through the heat exchangers and the tubing. Figure 11 shows the ring-down characteristic of the displacer piston in the presence of all the heat exchangers and tubing. The exponential envelope of the ring-down is a clear indication of the dominant viscous losses. This test yields an estimated power dissipation of 3.2 W at the nominal operating conditions. The energy-balance method indicates about 3.1 W of dissipated power for the same conditions.

Table 2 summarizes the estimated losses of the displacer, heat exchangers, and plumbing and compares them with the design calculations. There is a good agreement between calculations and estimated values for the fluid flow friction losses which validates all the adapted methodologies and computations. The computations for the heat exchangers are conservative, as expected. This may very well compensate for the unknown losses in other components, such as those due to bearing friction.

C. Power Piston

A ring-down test for the power piston while connected to the engine chamber confirms that the power piston resonates with the gas spring at a frequency of about 2.94 Hz.

A different ring-down test in which the power piston is separated from the engine chamber, and hence, is only linked to a weak magnetic spring enables estimation of the frictional losses. For this test, the ring-down oscillation frequency is low (about 0.8 Hz), and more uncertainties may prevail in the estimation. The frictional loss for the power piston is estimated to be 2.8 W in this test.

Gas hysteresis loss can be a significant source of dissipation for free-piston Stirling engines. This loss reduces the output work of the thermodynamic cycle and, in certain situations, can hinder the engine operation.[3] In order to characterize the gas hysteresis loss for the fabricated prototype, compression test is performed by actuating the power piston at its operating frequency. The actuation voltage is varied to achieve various piston strokes and, hence, compression ratios. At each operating point, using the energy-balance approach, one can estimate the power that is dissipated as gas hysteresis loss. Furthermore, the gas hysteresis loss can be estimated by calculating the area enclosed by the measured P-V loop at each operating point as well. The latter approach, adopted in this paper, includes the power piston seal leakage in the estimated value, which is expected not to exceed 1 W due to the tight clearance. Figure 12 depicts the experimental results of the compression test for the fabricated Stirling engine prototype. As expected from the theoretical model of the gas hysteresis phenomenon,[5] a quadratic function fits nicely to the measured data. This characteristic is used in the following section to estimate the gas hysteresis loss at the engine operating point.

Table 2. Comparison of the calculated component dissipations with the measurement-based estimations.

Component	P_{loss}^{calc}, W	$P_{loss}^{ring-down}$, W	$P_{loss}^{energy-balance}$, W
Piston only	$0.05 - 0.1$	0.5	0.76
Heat exchangers	$1.5 - 3.3$	1.1	0.49
Pipes and fittings	$0.5 - 2$	1.6	1.85
Total	$2.05 - 5.4$	3.2	3.1

V. Engine Operation

Figure 13 depicts the assembled Stirling engine test rig. The heater is heated by a voltage-controlled electric heater. The heating element passes through all the heater tubes. By varying the supply voltage of the heating element, one can adjust the input heat and hot side temperature. The metal tubes of the cooler are connected to a liquid cooling system. The coolant, ice-water in this case, flows through the tubes and removes heat from the engine working fluid as it passes through the heat exchanger fins.

As mentioned before, the displacer is driven by an inverter with adjustable frequency and amplitude. In order to minimize the required driving power, the displacer is driven at its resonant frequency. The voltage amplitude, on the other hand, is adjusted to drive the displacer at its full stroke.

The chamber pressure and power piston acceleration are monitored by appropriate sensing devices. By processing the acceleration data, one can obtain the power piston velocity and displacement signals. Displacement data will yield volume variation as all the dimensions are exactly known from the design records. Combining the pressure and volume signals, the P-V diagram of the thermodynamic cycle is obtained, which then characterizes the produced work.

The electric output of the power piston generator is connected to a resistive load. The voltage and current of the load are monitored as well. Therefore, the energy balance approach may be implemented here to assess the generated power.

Figures 14 and 15 show the measured pressure and volume variations as well as P-V characteristic of the engine while the thermocouples measure the working fluid temperatures of 175 °C and 25 °C in the vicinity of the heater and cooler, respectively, inside the engine chamber. The displacer piston operates at its full stroke while the power piston stroke is about 9.3 cm. The thermodynamic cycle output work based on the measured P-V characteristic is 13.1 W. Measurements, further confirm that about 7 W is delivered to the resistive load and 4 W is dissipated in the coils. Therefore, one can conclude that about 2.1 W is dissipated as the power piston frictional and eddy losses. Comparison of the measured data with simulation results, figure 2, indicates a good match for the pressure and volume amplitude variations. However, there is a mismatch in the phase angle of the P-V characteristic which, in turn, explains the difference of the measured and predicted (i.e., 23.8 W) output powers.

The fractional volumetric variation for the above operating conditions is about 0.114. The gas hysteresis characteristic of the engine, figure 12, suggests that 7 W of the cycle's output PV work is spent for the gas hysteresis loss. In addition, a small portion of the indicated output power is dissipated as enthalpy loss through the power piston clearance seal as well which, as mentioned before, is included in the gas hysteresis characteristic.

Note that the thermocouples in the experimental setup are located very close to the heat exchangers and they measure the working fluid temperature as it exits (or enters) the heat exchangers. Due to the heat leakage in the system, especially through the thin cylinder walls, the measured temperatures are probably higher than the actual average fluid temperatures that govern the thermodynamic cycle. This results in a higher output power prediction by the simulation program, which assumes adiabatic (or isothermal) compression and expansion spaces. Therefore, we conclude that the remainder 3.7 W of the dissipated must be in the form of enthalpy loss in the expansion space. A summary of the above discussion is tabulated in table 3.

Table 3. Power balance for the fabricated prototype at the operating point discussed in this paper.

Indicated power (adiabatic analysis)	23.8 W
Gas hysteresis loss	7 W
Expansion space enthalpy loss	3.7 W
Cycle output work	13.1 W
Bearing friction and eddy loss	2.1 W
Coil resistive loss	4 W
Power delivered to electric load	7 W

VI. Conclusion

Design, fabrication, and measurement results of a single-phase free-piston Stirling engine were presented in this paper. A very low-loss resonant displacer piston was designed for the system using a magnetic spring. Incorporating an array of permanent magnets, the magnetic spring had a very linear stiffness characteristic within the range of the displacer's stroke. The power piston was not mechanically linked to the displacer piston and formed a mass-spring resonating subsystem with the gas spring and had resonant frequency matched to that of the displacer.

The design of heat exchangers were discussed with an emphasis on their low fluid friction losses. The total power loss of the displacer piston, heat exchangers, and tubing at nominal conditions was measured at about 3.2 W that was well within the calculated range at design stage. The fabricated engine prototype was successfully tested and the experimental results were presented and discussed. Extensive experimentation on individual component subsystems confirmed the theoretical models and design considerations.

Acknowledgments

The authors would like to extend their gratitude to the National Science Foundation (award #ECS-0424462), for the financial support of the research presented in this paper. Also, they would like to thank Ben Lake and Joseph Gavazza of the Engineering Research Support Organization (ERSO) Machine Shop for their tremendous help in the design and fabrication of the prototype.

References

[1]Welford, W. T. and Winston, R., *High Collection Nonimaging Optics*, Academic Press, San Diego, CA, 1989.

[2]Senft, J. R., *An Introduction to Low Temperature Differential Stirling Engines*, Moriya Press, River Falls, WI, 5th ed., 2002.

[3]Der-Minassians, A., Aschenbach, K. H., and Sanders, S. R., "Low-Cost Distributed Solar-Thermal-Electric Power Generation," *Proceedings of SPIE*, Vol. 5185, 2004, pp. 89–98, Invited Paper.

[4]Der-Minassians, A. and Sanders, S. R., "Multiphase Free-Piston Stirling Engine for Solar-Thermal-Electric Power Generation Applications," *5th International Energy Conversion Engineering Conference, IECEC*, June 2007.

[5]Urieli, I. and Berchowitz, D. M., *Stirling Cycle Engine Analysis*, Adam Hilger Ltd, Bristol, 1984.

[6]Patt, P. J., "Design and Testing of a Coaxial Linear Magnetic Spring with Integral Linear Motor," *IEEE Trans. Magnetics*, Vol. 21, No. 5, September 1985, pp. 1759–1761.

[7]Qian, K., Zeng, P., Ru, W., and Yuan, H., "Novel Magnetic Spring and Magnetic Bearing," *IEEE Trans. Magnetics*, Vol. 39, No. 1, January 2003, pp. 559–561.

[8]Robertson, W., Cazzolato, B., and Zander, A., "A Multiple Array Magnetic Spring," *IEEE Trans. Magnetics*, Vol. 41, No. 10, October 2005, pp. 3826–3828.

[9]Kays, W. M. and London, A. L., *Compact Heat Exchangers*, McGraw-Hill, USA, 3rd ed., 1984.

[10]Kakac, S. and Liu, H., *Heat Exchangers, Selection, Rating, and Thermal Design*, CRC Press, Boca Raton, FL, 2nd ed., 2002.

[11]Thomas, B., "Evaluation of 6 Different Correlations for the Flow Friction Factor of Stirling Engine Regenerators," *Proceedings of the 34th Intesociety Energy Conversion Engineering Conference*, 1999.

[12]Thomas, B. and Pittman, D., "Update on the Evaluation of Different Correlations for the Flow Friction Factor and Heat Transfer of Stirling Engine Regenerators," *Proceedings of the 35th Intesociety Energy Conversion Engineering Conference*, Vol. 1, 2000, pp. 76–84.

[13]Tanaka, M., Yamashita, I., and Chisaka, F., "Flow and Heat Transfer Characteristics of the Stirling Engine Regenerator in an Oscillating Flow," *JSME International Journal*, Vol. 33, series II, No. 2, 1990, pp. 283–289.

[14]Zhao, T. S. and Cheng, P., "Oscillatory Pressure Drops Through a Woven-Screen Packed Column Subjected to a Cyclic Flow," *Cryogenics*, Vol. 36, No. 5, 1996, pp. 333–341.

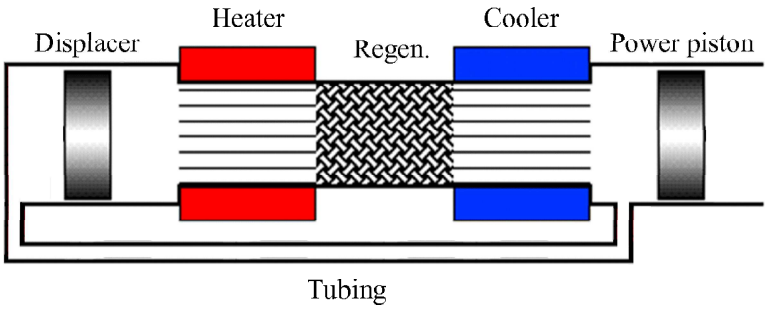

Figure 1. Schematic diagram of the designed Stirling engine.

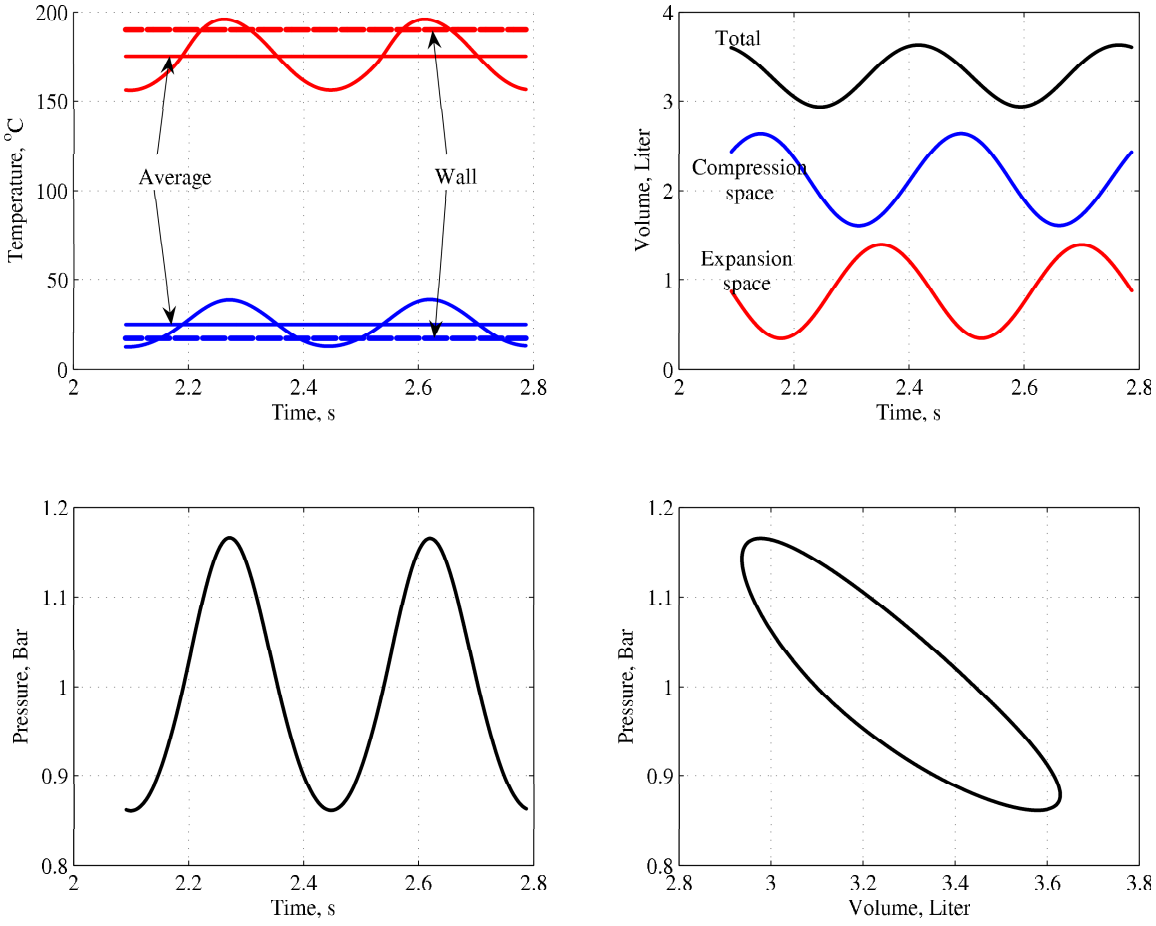

Figure 2. Simulation results of the single-phase free-piston Stirling engine thermodynamic behavior.

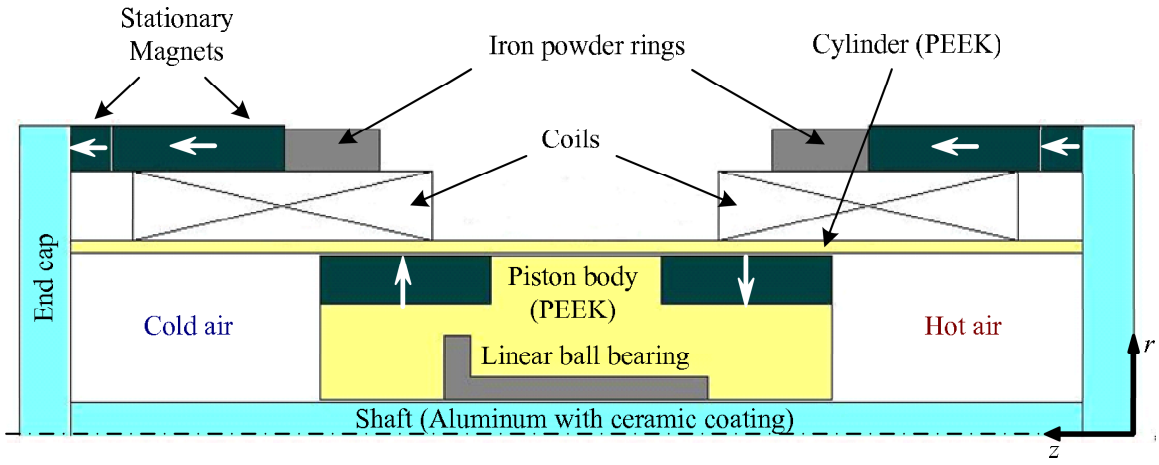

Figure 3. Schematic diagram of the displacer piston design.

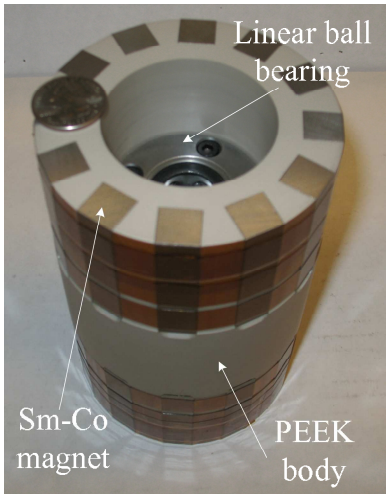

Figure 4. Fabricated displacer piston with embedded linear motion ball bearing and permanent magnet arrays.

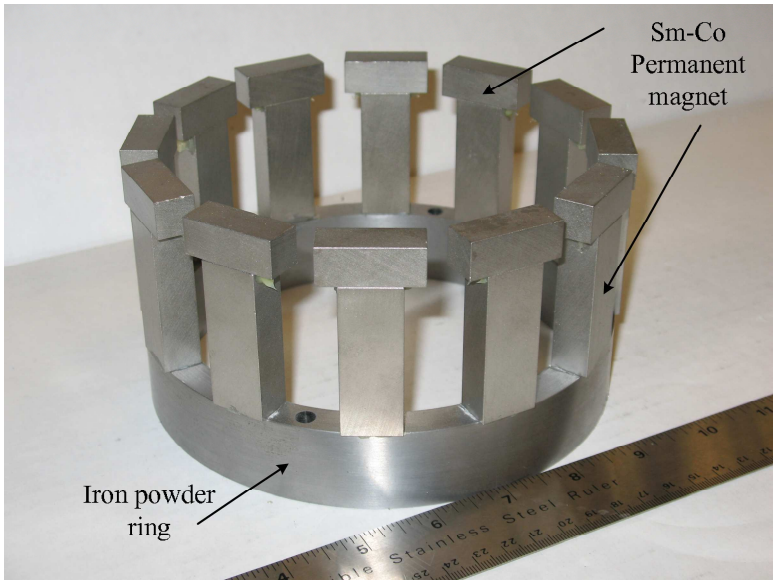

Figure 5. Stationary magnetic array that provides the linear spring function for the displacer.

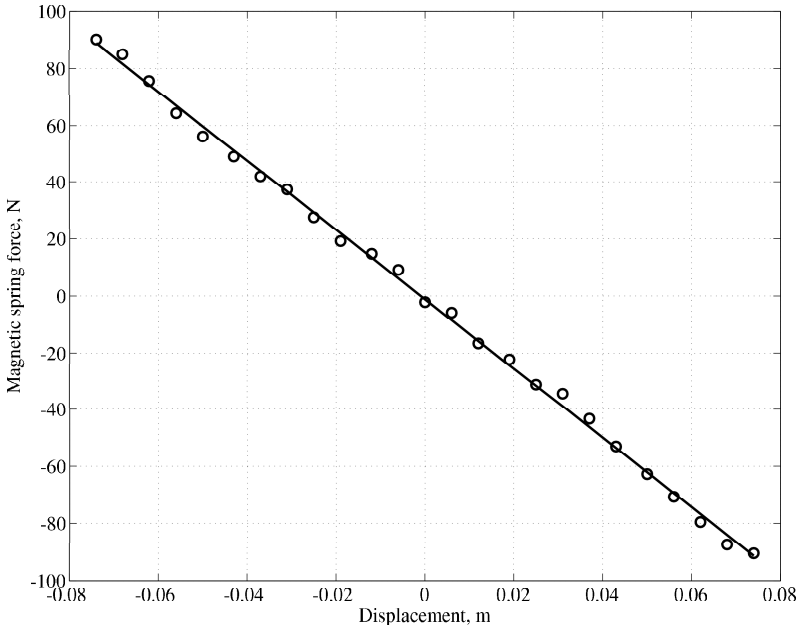

Figure 6. FEM analysis result for the stiffness characteristic of the magnetic spring. The straight line represents a linear regression fit through the data points (circles).

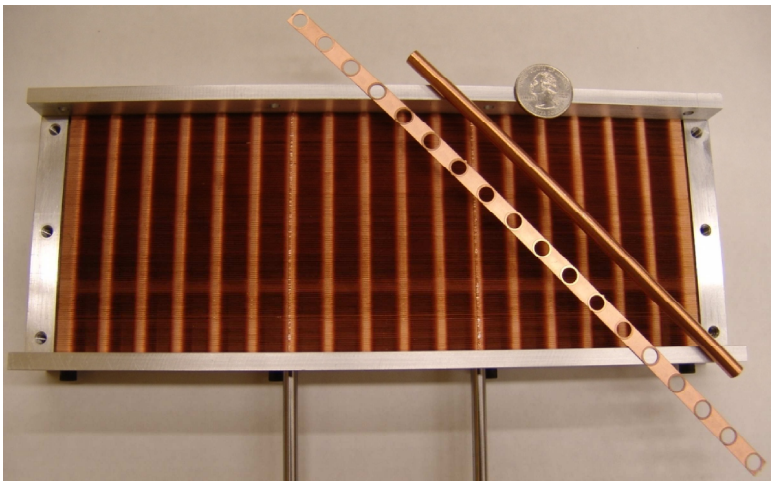

Figure 7. Fabricated heat exchanger shown with the etched fins and copper tube inserts.

Figure 8. Fabricated power piston shown with the low carbon steel body and Nd-Fe-B permanent magnets attached to one end.

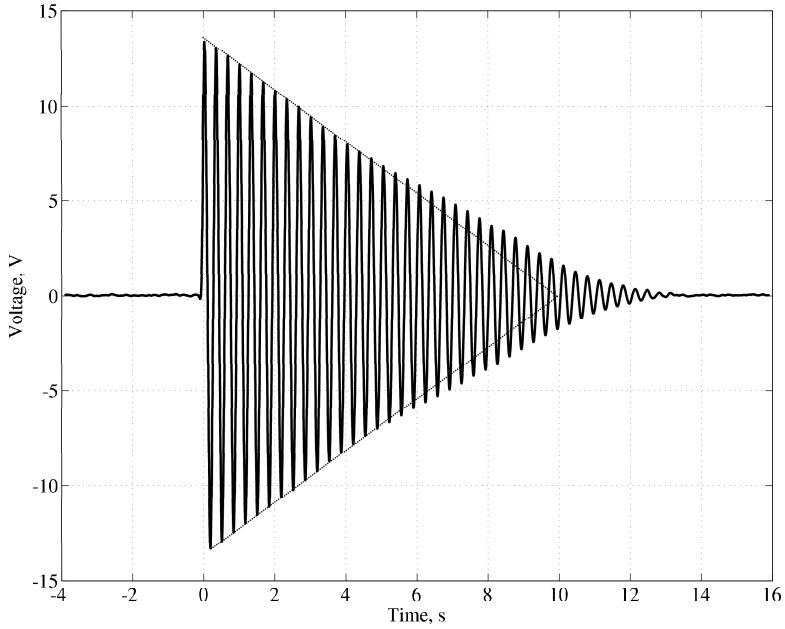

Figure 9. Ring-down characteristic of the displacer piston.

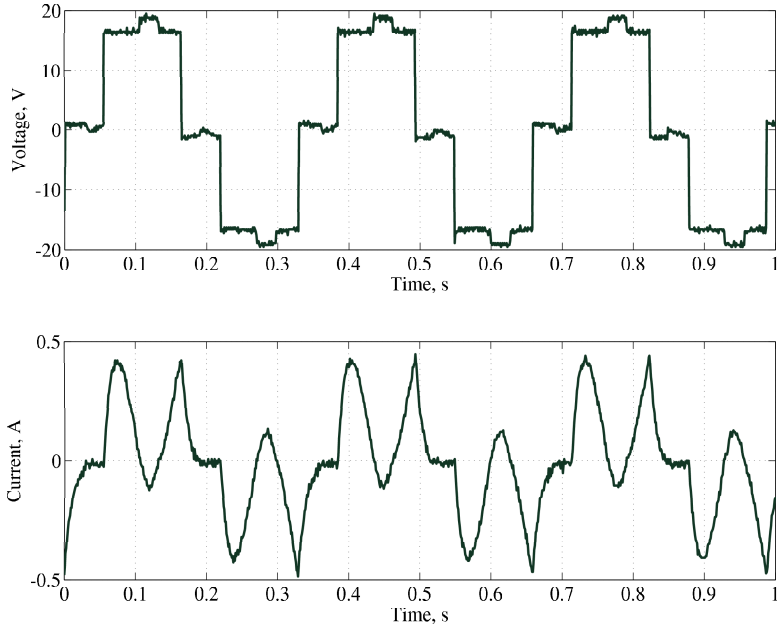

Figure 10. Input voltage and current waveforms of the displacer piston actuating coils at the resonant frequency (3 Hz) and naminal stroke.

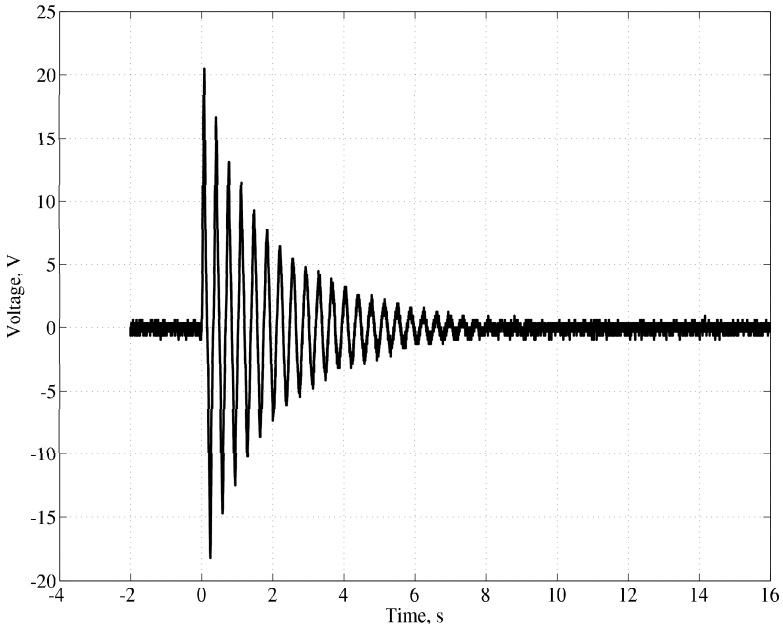

Figure 11. Ring-down characteristic of the displacer piston in the presence of the heater, cooler, regenerator, and the connecting pipes and fittings. Compare with figure 9.

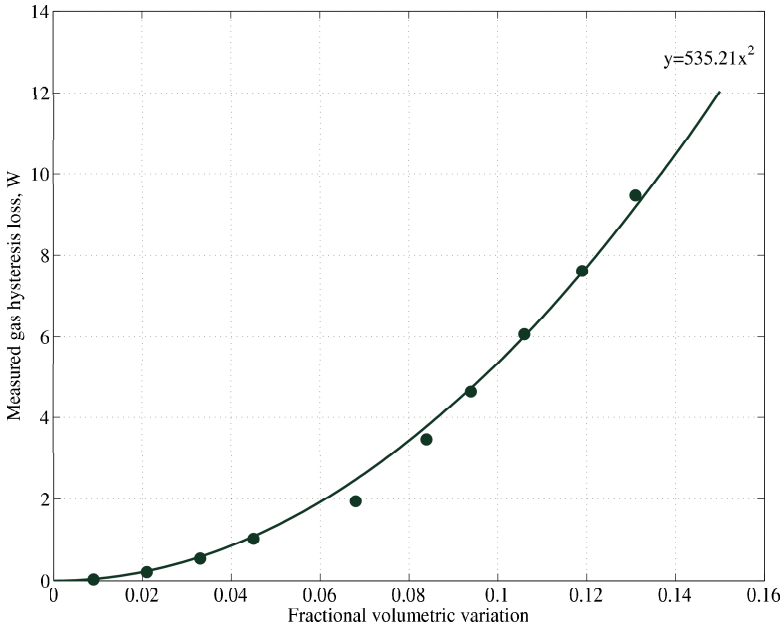

Figure 12. Gas hysteresis loss characteristic of the fabricated Stirling engine prototype.

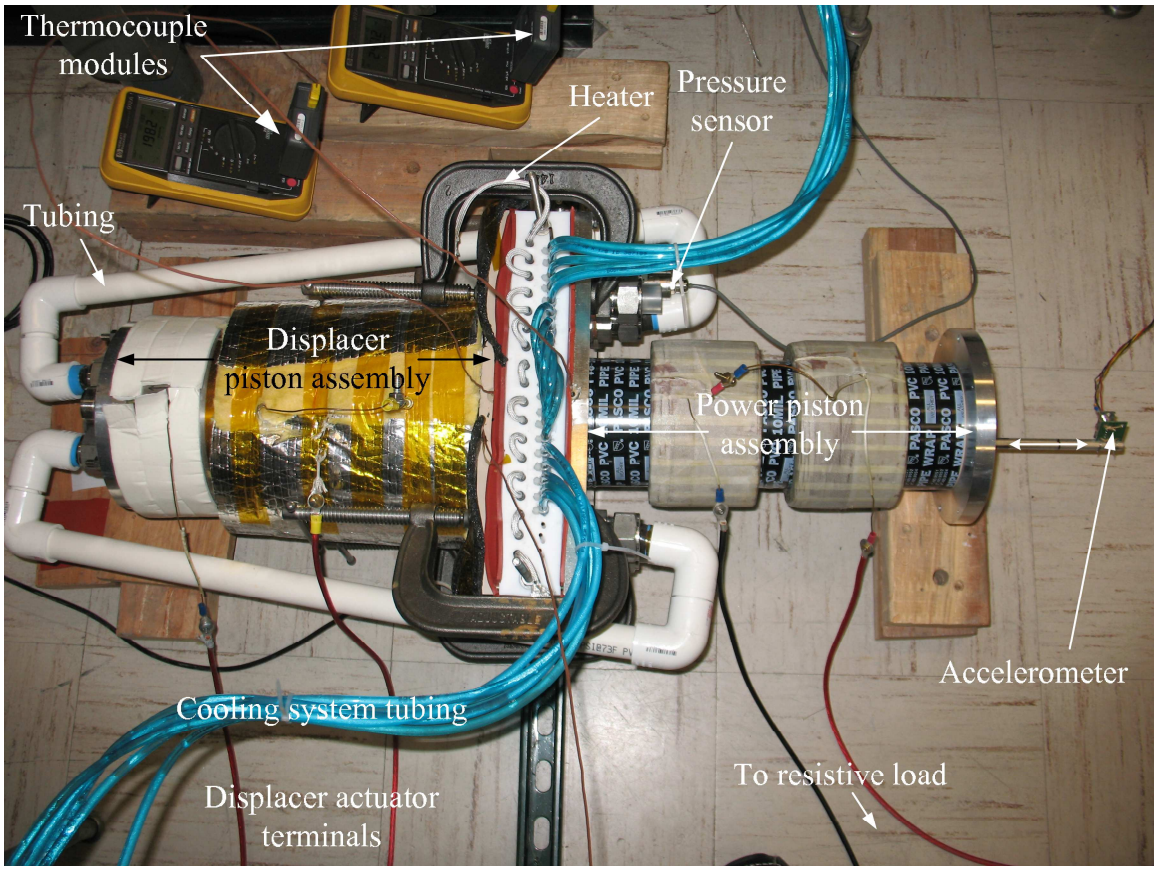

Figure 13. The Stirling engine experimental setup.

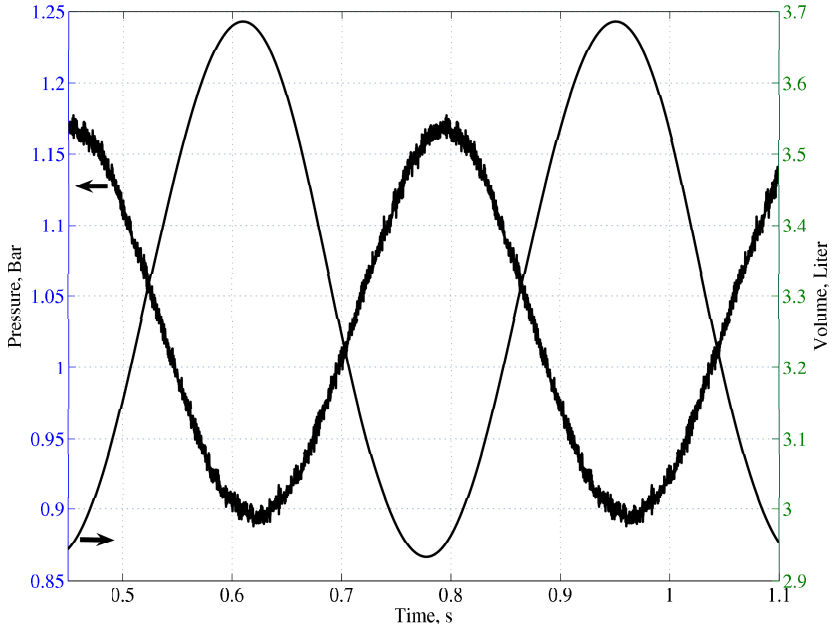

Figure 14. Measured engine pressure and volume variations.

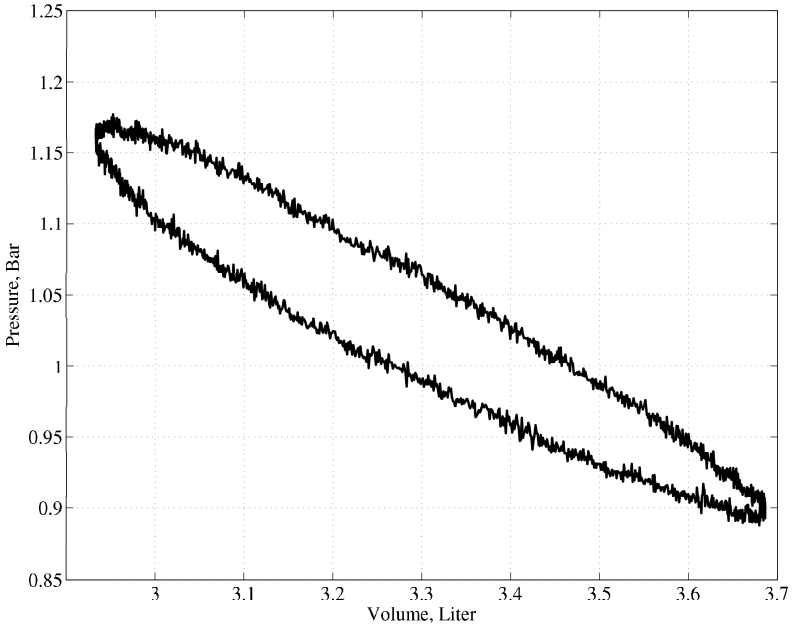

Figure 15. Measured PV diagram of the engine.